A&A 579, A31 (2015)
DOI: 10.1051/0004-6361/201526043

Astronomy & Astrophysics

Angular momentum redistribution by mixed modes in evolved low-mass stars

II. Spin-down of the core of red giants induced by mixed modes

K. Belkacem[1], J. P. Marques[2], M. J. Goupil[1], B. Mosser[1], T. Sonoi[1], R. M. Ouazzani[3], M. A. Dupret[4], S. Mathis[5,1], and M. Grosjean[4]

[1] LESIA, Observatoire de Paris, PSL Research University, CNRS, Université Pierre et Marie Curie, Université Denis Diderot, 92195 Meudon, France
e-mail: kevin.belkacem@obspm.fr
[2] Institut d'Astrophysique Spatiale, CNRS, Université Paris XI, 91405 Orsay Cedex, France
[3] Stellar Astrophysics Centre, Department of Physics and Astronomy, Aarhus University, Ny Munkegade 120, 8000 Aarhus C, Denmark
[4] Institut d'Astrophysique et de Géophysique, Université de Liège, Allée du 6 Août 17, 4000 Liège, Belgium
[5] Laboratoire AIM Paris-Saclay, CEA/DSM-CNRS-Université Paris Diderot; IRFU /SAp, Centre de Saclay, 91191 Gif-sur-Yvette Cedex, France

Received 6 March 2015 / Accepted 19 May 2015

ABSTRACT

The detection of mixed modes in subgiants and red giants by the CoRoT and *Kepler* space-borne missions allows us to investigate the internal structure of evolved low-mass stars, from the end of the main sequence to the central helium-burning phase. In particular, the measurement of the mean core rotation rate as a function of the evolution places stringent constraints on the physical mechanisms responsible for the angular momentum redistribution in stars. It showed that the current stellar evolution codes including the modelling of rotation fail to reproduce the observations. An additional physical process that efficiently extracts angular momentum from the core is thus necessary. Our aim is to assess the ability of mixed modes to do this. To this end, we developed a formalism that provides a modelling of the wave fluxes in both the mean angular momentum and the mean energy equations in a companion paper. In this article, mode amplitudes are modelled based on recent asteroseismic observations, and a quantitative estimate of the angular momentum transfer is obtained. This is performed for a benchmark model of 1.3 $M_{\odot}$ at three evolutionary stages, representative of the evolved pulsating stars observed by CoRoT and *Kepler*. We show that mixed modes extract angular momentum from the innermost regions of subgiants and red giants. However, this transport of angular momentum from the core is unlikely to counterbalance the effect of the core contraction in subgiants and early red giants. In contrast, for more evolved red giants, mixed modes are found efficient enough to balance and exceed the effect of the core contraction, in particular in the hydrogen-burning shell. Our results thus indicate that mixed modes are a promising candidate to explain the observed spin-down of the core of evolved red giants, but that an other mechanism is to be invoked for subgiants and early red giants.

Key words. waves – stars: evolution – stars: oscillations – stars: interiors – stars: rotation

1. Introduction

The CoRoT (Baglin et al. 2006a,b; Michel et al. 2008) and *Kepler* (Borucki et al. 2010) space-borne missions provided a wealth of observed stars exhibiting solar-like oscillations, from the main-sequence to the red-giant phases (see Chaplin & Miglio 2013, for a review). A large number of those stars are low-mass evolved stars showing a rich spectrum of mixed modes, which behave as acoustic modes in the stellar envelope and as gravity modes in the core. They are therefore detectable at the stellar surface while yielding information on the innermost regions (e.g., Dziembowski 1971; Scuflaire 1974; Aizenman et al. 1977; Dziembowski et al. 2001; Dupret et al. 2009).

While mixed modes allowed unveiling the structure of the red giants core (Bedding et al. 2011; Mosser et al. 2011, 2014), the detection of associated rotational splittings enabled measuring the mean core rotation of subgiant and red giant stars (Beck et al. 2012; Deheuvels et al. 2012, 2014; Mosser et al. 2012b). It turns out that the core of low-mass red giant stars slows down during evolution. Since local conservation of angular momentum would imply a spin-up of the core, these observations indicate a strong transfer of angular momentum from the inner to the outer layers of these stars. However, current stellar evolutionary rotating models that take the transport of angular momentum into account fail to reproduce the observations. Meridional circulation or shear instabilities are not efficient enough to slow down the red-giant cores (e.g., Eggenberger et al. 2012; Marques et al. 2013; Ceillier et al. 2013), and recent attempts to include the effect of propagative internal gravity waves (Fuller et al. 2014) or magnetic fields using the Taylor-Spruit dynamo formalism (Cantiello et al. 2014) failed to solve the problem. Nonetheless, for subgiants and early red giants, Rüdiger et al. (2015) have recently shown that magneto-rotational instabilities of a toroidal magnetic field could explain the angular momentum redistribution in subgiants and early red giants (see also Maeder & Meynet 2014).

Hence, an additional physical mechanism that efficiently extracts angular momentum from the core of red giants seems to be

needed. Non-radial modes in subgiants and red giants are potential candidates. Indeed, prograde and retrograde mixed modes are differentially damped in the presence of rotation, allowing a net transport of angular momentum (e.g., Ando 1986; Lee & Saio 1993). Our aim is thus to investigate the ability of mixed modes to transfer angular momentum from the inner radiative interior to the outer convective layers.

In the first article of this series (Belkacem et al. 2015, hereafter Paper I), we used the transformed Eulerian mean (TEM) formalism to account for the effect of wave driving through both the wave momentum flux in the mean angular momentum equation and the wave heat flux in the mean energy equation. The wave field was then modelled using the asymptotic, quasi-adiabatic, and slow-rotation approximations, valid in the dense radiative layers of evolved stars. This allowed us to obtain an explicit expression of the wave fluxes appearing in the mean angular momentum and energy equations. This article, the second of this series, is dedicated to a quantitative determination of the angular momentum transported by mixed modes, which requires the knowledge of mode amplitudes. Recent CoRoT and *Kepler* observations (Baudin et al. 2011; Mosser et al. 2012a; Samadi et al. 2012) allow us to determine mixed-mode amplitudes and subsequently to determine the efficiency of angular momentum transport by mixed modes.

The paper is organized as follows: Sect. 2 recalls the formalism developed in Paper I, while Sect. 3 presents the modelling of the equilibrium models and related oscillations. In Sect. 4, based on the observations, we describe the modelling of mode amplitudes. Finally, the estimate of the angular momentum transport efficiency is presented in Sect. 5, and Sect. 6 is dedicated to discussions and conclusions.

2. Theoretical formalism

In this section, we recall the formalism developed in Paper I as well as the related assumptions for both the mean flow and the wave fluxes appearing in the mean equations.

2.1. Mean flow equations

Following Paper I, we adopt the transformed Eulerian mean formalism (TEM). In addition, we assume shellular rotation (see Maeder 2009, for an extensive discussion) so that at dominant order the mean angular momentum equation is

$$\langle\rho\rangle \frac{\mathrm{d}\left(r^2\Omega_0\right)}{\mathrm{d}t} = -\frac{1}{r^2}\frac{\partial}{\partial r}\left[r^2\left(\mathcal{F}_{\rm circ}+\mathcal{F}_{\rm shear}+\mathcal{F}_{\rm waves}\right)\right], \tag{1}$$

where Ω_0 is the rotation angular frequency that depends only on the radius, ρ is the density, the overbar and the symbol $\langle\rangle$ denotes the horizontal average (i.e. azimuthal and meridional). The fluxes are defined by

$$\mathcal{F}_{\rm circ} = -\frac{1}{5}\langle\rho\rangle r^2\Omega_0 U_2^{\dagger}, \tag{2}$$

$$\mathcal{F}_{\rm shear} = -\langle\rho\rangle \nu_{\rm v} r^2 \frac{\partial\Omega_0}{\partial r}, \tag{3}$$

$$\mathcal{F}_{\rm waves} = \langle\rho\rangle\left\langle \varpi\left[\overline{v'_\phi v'_{\rm r}} + 2\cos\theta\,\Omega_0\,\overline{v'_\theta s'}\left(\frac{\mathrm{d}\langle s\rangle}{\mathrm{d}r}\right)^{-1}\right]\right\rangle, \tag{4}$$

where $\varpi = r\sin\theta$, the overbar is the azimuthal average, $U_2^{\dagger}$ is the residual meridional velocity, ν_v is the radial eddy viscosity, s is the specific entropy, and the prime denotes perturbations associated with the non-radial oscillations, so that v'_ϕ, $v'_{\rm r}$, v'_θ are the azimuthal, radial, and meridional component of the wave velocity field, and s' the wave Eulerian perturbation of entropy. We have also introduced the Lagrangian derivative $\mathrm{d}/\mathrm{d}t = \partial/\partial t + \dot{r}\,\partial/\partial r$.

Under the same assumptions as for Eq. (1), the mean entropy equation is

$$\langle\rho\rangle \frac{\mathrm{d}\langle s\rangle}{\mathrm{d}t} = -\frac{1}{r^2}\frac{\partial}{\partial r}\left\langle r^2\,\mathcal{S}\right\rangle + \langle Q\rangle \tag{5}$$

with

$$\mathcal{S} = \langle\rho\rangle\,\overline{s'\,v'_{\rm r}}, \tag{6}$$

and

$$\langle T\rangle\langle Q\rangle = \langle\rho\varepsilon\rangle + \frac{1}{r^2}\frac{\partial}{\partial r}\left(r^2\langle\chi\rangle\frac{\partial\langle T\rangle}{\partial r}\right), \tag{7}$$

where T is the temperature, ε is the nuclear energy generation rate and χ is the thermal conductivity (see, e.g., Sect. 6 of Mathis & Zahn 2004, and also Maeder & Zahn 1998). This expresses energy conservation on level surfaces.

To quantify the effect of the waves on the rotation profile, we further need to provide a modelling of the wave field[1].

2.2. Wave flux modelling

Our aim is to determine the angular momentum redistribution induced by mixed modes in the radiative region of low-mass evolved stars. Therefore, the wave fluxes in Eqs. (1) and (5) must be modelled. This has been done in Paper I, so that for the momentum equation we have

$$-\frac{1}{r^2}\frac{\partial}{\partial r}\left(r^2\mathcal{F}_{\rm waves}\right) = \sum_{\ell,m} a^2_{\ell,m}\left(\mathcal{A}^m_\ell\frac{\partial^2\left(r^2\Omega_0\right)}{\partial r^2} + \mathcal{B}^m_\ell\frac{\partial\left(r^2\Omega_0\right)}{\partial r} + C^m_\ell\,\Omega_0 + m\hat{\sigma}\mathcal{D}^m_\ell\right), \tag{8}$$

where the coefficients $\mathcal{A}^m_\ell, \mathcal{B}^m_\ell, C^m_\ell, \mathcal{D}^m_\ell$ are given by Eqs. (A.25) to (A.28) of Paper I, and $\hat{\sigma} = \sigma_{\rm R} + m\Omega_0$ (with $\sigma_{\rm R}$ the modal frequency). The amplitude $a_{\ell,m}$ corresponds to the amplitude of a mode of a given angular degree, ℓ, and azimuthal order, m. We note that the amplitude is considered statistically constant in time since we deal with solar-like oscillations that result from a balance between mode driving and damping (see Samadi 2011, for details).

For the entropy equation, we obtained

$$\frac{1}{r^2}\frac{\partial}{\partial r}\left\langle r^2\,\mathcal{S}\right\rangle = \sum_{\ell,m}\frac{a^2_{\ell,m}}{2r^2}\frac{\partial}{\partial r}\left(r^2\,\rho\,\alpha\frac{\mathrm{d}s}{\mathrm{d}r}k_r^2\,|\xi_r^{\ell,m}|^2\right), \tag{9}$$

where

$$\alpha = -\frac{L}{4\pi r^2\rho T}\left(\frac{\nabla_{\rm ad}}{\nabla}-1\right)\left(\frac{\mathrm{d}s}{\mathrm{d}r}\right)^{-1}$$

$$k_r^2 \simeq \frac{\ell(\ell+1)}{r^2}\left(\frac{N^2}{\sigma_{\rm R}^2}-1\right), \tag{10}$$

with L the luminosity, N the buoyancy frequency, ∇ and $\nabla_{\rm ad}$ the actual and adiabatic temperature gradients, respectively, and

[1] In this article, by wave we denote global mixed modes.

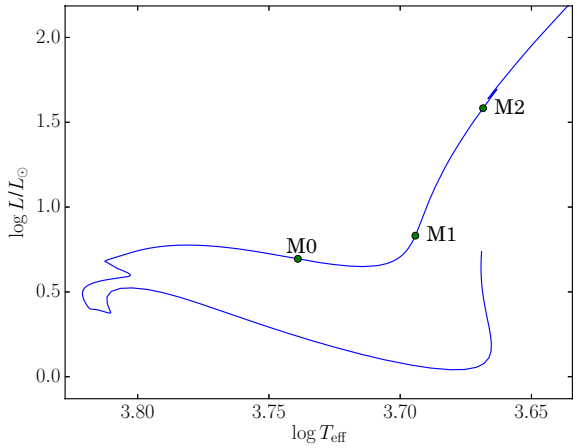

Fig. 1. Evolutionary track on the Hertzsprung-Russell (HR) diagram of a 1.3 $M_\odot$ model, showing the location of the selected models (see Sect. 3 for details).

$\xi_r^{\ell,m}$ the radial component of the eigenfunction for a mode of angular degree ℓ and azimuthal order m. The overbars and angular brackets have been dropped for ease of notation.

We also recall that in the course of deriving Eqs. (8) and (9) several simplifying approximations were performed, namely:

1. *The quasi-adiabatic approach*: it consists of neglecting the difference between adiabatic and non-adiabatic eigenfunctions in the full wave equations. This approximation is valid provided the local thermal timescale is much longer than the modal period. This is justified in the radiative region of evolved low-mass stars.
2. *The low-rotation limit*: we consider the low-rotation limit in the radiative regions or, more precisely, $\sigma_{\rm R} \gg \Omega_0$. This is justified by recent inferences of the rotation rate in the core of subgiants (Deheuvels et al. 2012, 2014) and red giants (Mosser et al. 2012b) using seismic constraints from *Kepler*.
3. *The asymptotic limit*: we used an asymptotic description for gravity modes (e.g., Dziembowski et al. 2001; Godart et al. 2009), which is valid for mixed modes in the inner radiative region of subgiants and red giants (e.g., Goupil et al. 2013).

Consequently, our formalism is valid in the dense radiative core of evolved slowly rotating stars.

3. Computing selected stellar models

We have computed an evolutionary sequence of a benchmark model of a 1.3 $M_\odot$ evolved low-mass star representative of CoRoT and *Kepler* observations. We selected three $M = 1.3\ M_\odot$ models at three post-main sequence stages of this evolutionary sequence, as discussed below. The location of the models in the Hertzsprung-Russell (HR) diagram is shown in Fig. 1, and their characteristics are summarised in Table 1.

3.1. Equilibrium models and related eigenfunctions and eigenfrequencies

We used the stellar evolution code CESTAM (Marques et al. 2013) to compute the equilibrium models. The atmosphere was computed assuming a grey Eddington approximation. Convection was included according to Canuto et al. (1996), with a mixing-length parameter $\alpha = 0.67$. The initial chemical composition follows Asplund et al. (2005), with a helium mass fraction of $Y = 0.261$ and a metallicity of $Z = 0.0138$. We used the OPAL equation of state (Rogers et al. 1996) and opacities (Iglesias & Rogers 1996), complemented, at $T < 10^4$ K, by the Alexander & Ferguson (1994) opacities. We adopted the NACRE nuclear reaction rates from Angulo et al. (1999) except for the ^{14}N + p reaction, where we used the reaction rates given in Imbriani et al. (2004).

Finally, we used the ADIPLS code to compute adiabatic oscillations (Christensen-Dalsgaard 2008, 2011), that is, to obtain the eigenfunctions and eigenfrequencies.

Table 1. Characteristics of the selected models as described in Sect. 3.

Model	Age (Myr)	$R/R_\odot$	$L/L_\odot$	$\Delta\nu$ (μHz)	$\nu_{\rm max}$ (μHz)
M0	4401	2.47	4.95	39.5	666
M1	4590	3.55	6.78	22.9	339
M2	4791	9.51	38.3	5.24	48.8

Notes. Model M0 is a subgiant, model M1 is at the base of the red-giant branch, and model M2 is a red giant. Here, $\Delta\nu$ is the large separation and $\nu_{\rm max}$ is the frequency at the maximum height of the oscillation power spectrum.

Table 2. Parameters of the synthetic profiles as described in Sect. 3.2 (see also Eq. (11)).

Model	$\Omega_{\rm C}/2\pi$ (nHz)	$\Omega_{\rm S}/2\pi$ (nHz)	$r_{\rm t}/R_{\rm star}$	$w/R_{\rm star}$
M0	600	200	0.1452	1.452×10^{-1}
M1	1000	55	1.009×10^{-2}	1.211×10^{-3}
M2	500	8.1	3.316×10^{-3}	3.015×10^{-4}

3.2. Rotation profiles

We consider that rotation has negligible effects on the equilibrium structure of the star and that it can be considered as a perturbation for the oscillations. This approximation is consistent with the formalism developed in Paper I.

The rotation profiles are therefore determined by computing synthetic profiles that match the observations. The synthetic profiles should have a core that rotates faster than the envelope, with a transition region located at the H-burning shell in the case of red giant stars (models M1 and M2). The width of the transition region is related to the width of the H-burning shell. We consequently used the following profile

$$\Omega(r) = \Omega_{\rm S} + \frac{\Omega_{\rm C} - \Omega_{\rm S}}{2}\left[1 + {\rm erf}\left(\frac{r_{\rm t} - r}{w}\right)\right], \qquad (11)$$

where $\Omega_{\rm S}$ and $\Omega_{\rm C}$ are the surface and central angular velocities, respectively, and $r_{\rm t}$ and w are the radius and width of the burning shell. $\Omega_{\rm C}$ was chosen to reproduce the mean core rotation rate of evolved low-mass stars as derived from *Kepler* observations (see Mosser et al. 2012b; Deheuvels et al. 2014, and the surface rotation rate ($\Omega_{\rm S}$) was obtained so as to conserve the total angular momentum from the subgiant stage (model M0).

For the subgiant model (model M0), we also used Eq. (11), but with both $r_{\rm t}$ and w given by the radius of the central convective zone at the end of the main sequence (just before it disappears). In this case, the central and surface rotation ($\Omega_{\rm C}$ and $\Omega_{\rm S}$, respectively) were chosen to reproduce the results of Deheuvels et al. (2012). The values of the parameters for models M0, M1, and M2 are summarised in Table 2, and the resulting rotation profiles are displayed in Fig. 2.

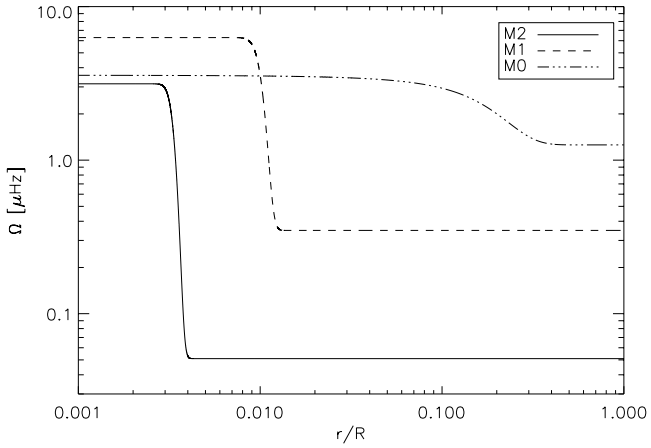

Fig. 2. Synthetic rotation profiles, computed as described in Sect. 3.2, for models M0, M1, and M2 as a function of the radius normalised by the total radius. We used logarithmic scales.

4. Modelling mode amplitudes

There are mainly two approaches to compute mode amplitudes. The first is based on a full non-adiabatic computation including a time-dependent treatment of convection. This procedure is time-consuming, however, and still suffers from theoretical uncertainties (see Dupret et al. 2009; Grosjean et al. 2014, for details). The second is based on recent CoRoT and *Kepler* observations that allowed us to measure the amplitudes of solar-like modes in a wide variety of stars in different evolutionary stages. This wealth of observations made it possible to establish scaling relations that provide mode amplitudes versus global stellar parameters (e.g., Mosser et al. 2012a; Samadi et al. 2012). In this paper, we adopt the latter approach.

4.1. Radial mode amplitudes

We first express the amplitudes of radial modes. The surface velocity of the radial modes, at the frequency of maximum height ($\nu_{\rm max}$) in the oscillation power spectrum, follows the scaling relation (see Belkacem & Samadi 2013, for details)

$$\frac{V_{\ell=0}\left(\nu=\nu_{\rm max}\right)}{V_{\ell=0,\odot}\left(\nu=\nu_{\rm max}\right)} \approx \left(\frac{T_{\rm eff}}{T_{\odot,\rm eff}}\right)^{-1.77} \left(\frac{\nu_{\rm max}}{\nu_{\odot,\rm max}}\right)^{-1.15} \left(\frac{\Delta\nu}{\Delta\nu_{\odot}}\right)^{0.65}, \quad (12)$$

where $T_{\rm eff}$ is the effective temperature, $\Delta\nu$ is the large separation, and the $\odot$ symbols stand for the solar values. Here we adopt the values $T_{\odot,\rm eff} = 5777$ K, $\nu_{\odot,\rm max} = 3050\,\mu$Hz, and $\Delta\nu_{\odot} = 135\,\mu$Hz.

To account for the frequency dependence of radial mode amplitudes, we follow the work of Mosser et al. (2010) , who used a Gaussian envelope centred on $\nu_{\rm max}$ with a full-width at half-maximum $\delta\nu_{\rm env}$, that is,

$$V^2_{\ell=0}\left(\nu\right) = V^2_{\ell=0}\left(\nu=\nu_{\rm max}\right)\ {\rm e}^{-(\nu-\nu_{\rm max})^2/(2\sigma^2)}, \quad (13)$$

with $\sigma = \delta\nu_{\rm env}/(2\sqrt{2\ln 2})$. Based on *Kepler* observations, we take $\delta\nu_{\rm env} = 150\,\mu$Hz for M0, $\delta\nu_{\rm env} = 70\,\mu$Hz for M1, and $\delta\nu_{\rm env} = 30\,\mu$Hz for M2 for the following.

4.2. Non-radial mode amplitudes

The next step is to consider the amplitudes of non-radial modes. The ratio between radial and non-radial mode amplitudes of comparable frequencies can be written as (see Benomar et al. 2014, for details)

$$\frac{V^2_{\ell}\left(\nu\right)}{V^2_{\ell=0}\left(\nu\right)} \approx \frac{\mathcal{M}^2_{\ell=0}}{\mathcal{M}^2_{\ell}} \frac{\Gamma_{\ell=0}}{\Gamma_{\ell}}, \quad (14)$$

where $\mathcal{M}_{\ell} = \int \boldsymbol{\xi}^2 {\rm d}m/\xi^2(R)$ is the mode mass, $\boldsymbol{\xi}$ is the eigenfunction, m is the mass profile, R is the total radius, and Γ_{ℓ} is the mode linewidth that is related to the mode damping rate η_{ℓ} by $\Gamma_{\ell} = \eta_{\ell}/\pi$.

For high angular degrees, the radiative work of the oscillations in the innermost regions dominantes the work done in the uppermost layers (see Grosjean et al. 2014, for details). It follows that the mode amplitudes of high angular degrees become very small due to strong radiative damping. We thus define a cut-off angular degree, $\ell_{\rm max}$, below which we assume that the work of non-radial modes equals the work of radial modes

$$\Gamma_{\ell=0}\mathcal{M}_{\ell=0} = \mathcal{M}_{\ell\leq\ell_{\rm max}}\Gamma_{\ell\leq\ell_{\rm max}} \quad (15)$$

where the product between the mode mass and the mode damping rate equals the work integral (e.g., Dupret et al. 2009; Benomar et al. 2014; Grosjean et al. 2014). Now, using Eq. (15) together with Eq. (14) leads to

$$\frac{V^2_{\ell\leq\ell_{\rm max}}\left(\nu\right)}{V^2_{\ell=0}\left(\nu\right)} \approx \frac{\mathcal{M}_{\ell=0}}{\mathcal{M}_{\ell\leq\ell_{\rm max}}}. \quad (16)$$

For $\ell > \ell_{\rm max}$, we assume that the radiative damping in the innermost region becomes dominant over the damping of the upper layers so that mode amplitudes become negligible.

The cut-off angular degree is obtained by assuming that the work done over an oscillation period through the effect of radiative losses in the innermost layers becomes of the same order of magnitude as the work done in the uppermost layers. We obtain $\ell_{\rm max} = 6$ for M0, $\ell_{\rm max} = 4$ for M1, and $\ell_{\rm max} = 2$ for M2 (see Appendix A for details). Note that this approach for the modelling of mode amplitudes provides a lower limit to the amount of angular momentum transported by mixed modes since we neglect the contribution of angular degrees higher than $\ell_{\rm max}$. However, this is enough to determine whether mixed modes are able to slow down the rotating core of red giants.

Finally, we assume that the relation between the surface mode velocity and the mode amplitude is given by $V^2_{\ell} = a^2_{\ell,m}\sigma^2_{\rm R}|\boldsymbol{\xi}_{\ell}|^2/2$ (see Samadi 2011). The results obtained for mode amplitudes of angular degrees $\ell = \{0, 1, 2\}$ are presented in Fig. 3 for the three models M0, M1, and M2, described in Sect. 3.

5. Quantitative estimate of angular momentum extracted by mixed modes

Our aim is to estimate the rate of angular momentum transported by mixed modes for the benchmark models M0, M1, and M2. To this end, as in Paper I, we introduce the notation

$$\dot{j} = -\frac{1}{r^2}\frac{\partial}{\partial r}\left(r^2\mathcal{F}_{\rm waves}\right), \quad (17)$$

where the right-hand side is given by Eq. (8). Using the approach presented in Sect. 4 to derive the amplitudes, we compute the wave fluxes in the right-hand side of Eqs. (1) and (5) using Eqs. (8) and (9).

The contribution of the mixed modes to the mean angular momentum equation is shown in Fig. 4 for models M0, M1,

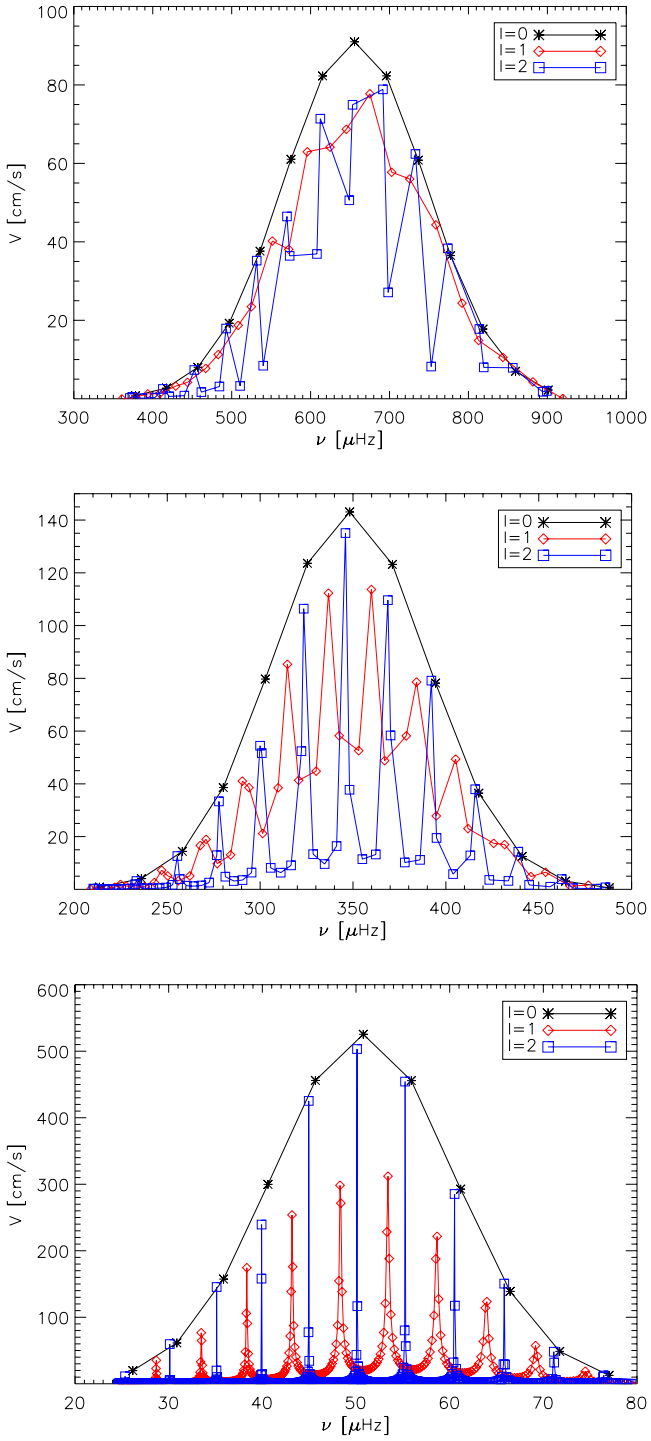

Fig. 3. Mode amplitudes versus mode frequencies for models M0 (*top panel*), M1 (*middle panel*), and M2 (*bottom panel*). The amplitudes are computed as described in Sect. 4.

and M2. The main effect of mixed modes is to slow down the core of the stars in the region near the maximum of the buoyancy frequency that also corresponds to the edge of the fast rotating core. For the red-giant models, this region is the hydrogen-burning shell. The decrease shown towards the upper radiative layers is the result of both a lower rotation rate and a lower value of the buoyancy frequency. This behaviour is similar in the three models. In addition, the amount of angular momentum extracted by mixed modes hardly depends on the rotation gradient

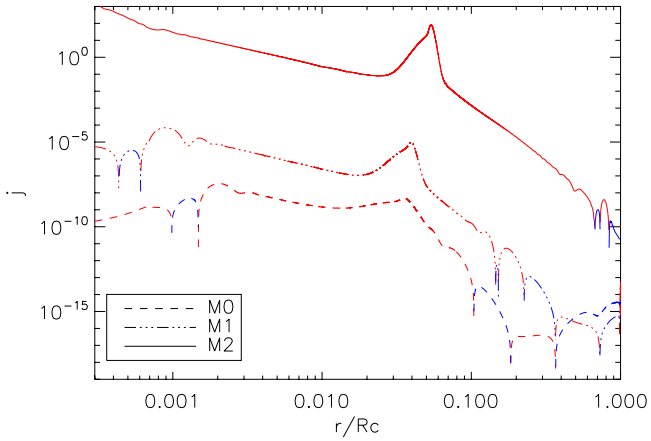

Fig. 4. Rate of temporal variation of the mean specific angular momentum ($\dot{J}$ as defined by Eq. (17)) as a function of the star radius normalised by the radius of the base of the convective envelope. Red corresponds to $\dot{J} < 0$ and blue to $\dot{J} > 0$.

between the core and the envelope (the sensitivity of the results to the parameter w in Eq. (11) remains weak).

The amount of angular momentum extracted by mixed modes increases with the evolutionary stage of the star. This effect is the result of several factors. First, as shown in Fig. 3, mode amplitudes increase from models M0 to M2 and thus more energy is available to transport angular momentum. Moreover, the buoyancy frequency also increases and so does the radial wave number in the gravity-mode cavity. As the energy exchanges between modes and the background is proportional to the radial wave number, the amount of angular momentum extracted also increases. Finally, the number of mixed modes between two p-dominated modes significantly increases between M0 and M2.

Furthermore, the angular momentum is mainly carried away by g-dominated modes of the highest angular degrees. Indeed, these modes are very efficiently trapped in the core and undergo a larger radiative damping (due to the larger radial wave number). The predominance of high angular degree modes implies that $\dot{J}$ is sensitive to our determination of $\ell_{\max}$. As mentioned before, the estimate of the amount of angular momentum extracted in the radiative regions is thus a lower limit. In other words, adding the contribution of angular degrees higher than $\ell_{\max}$ would strengthen these trends.

To proceed and assess the efficiency of the transport of angular momentum for our benchmark models, we compare two timescales, namely:

– the timescale associated with the efficiency of the transport of angular momentum by mixed modes, defined as

$$T_m^{-1} = \left| \frac{\dot{J}}{\rho r^2 \Omega_0} \right|, \tag{18}$$

– the timescale associated with the contraction of the star, defined as

$$T_c^{-1} = \left| -\frac{1}{\rho r^4 \Omega_0} \frac{\partial}{\partial r} \left(\rho r^4 \Omega_0 \, \dot{r} \right) \right| \approx \left| -\frac{\dot{r}}{r} \right|, \tag{19}$$

where $\dot{r} = \mathrm{d}r/\mathrm{d}t$.

The two timescales are shown in Fig. 5 (top panel). In all the radiative regions of models M0 and M1, the extraction of angular momentum remains negligible compared to the star contraction.

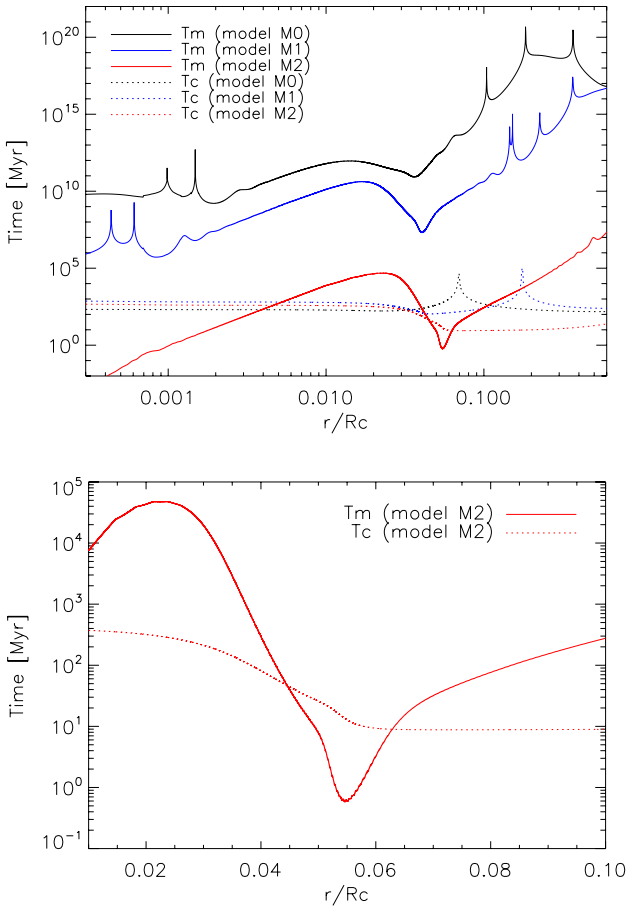

Fig. 5. *Top panel*: timescales versus normalised radius (i.e., normalised by the radius of the base of the convective envelope) for models M0, M1, and M2. The solid lines correspond to the timescale associated with the transport of angular momentum by mixed modes (see Eq. (18)) and the dotted lines correspond to the timescale associated with the contraction of the star (see Eq. (19)). *Bottom panel*: same as the top panel, except that only a zoom for model M2 is shown.

In contrast, for model M2, the timescale of angular momentum extraction is of the same order of magnitude as the contraction timescale and even lower in the hydrogen-shell-burning region, for which the contraction is maximal (see Fig. 5, bottom panel). However, in the very centre or in the upper radiative region, the mixed mode extraction of angular momentum is again negligible.

Therefore, we conclude that the extraction of angular momentum by mixed modes is negligible in subgiants and early red giants, but becomes strong in the hydrogen-burning shell in stars higher on the red-giant branch. In these cases, mixed modes are able to counterbalance the spin-up due to the star contraction and can thus enforce a spin-down in those layers. We note, however, that the exact location in the HR diagram of the transition between inefficient and efficient extraction by mixed modes is likely to depend on the mass and internal physics of the models.

6. Concluding remarks

Based on the theoretical formalism developed in Paper I, we computed the amount of angular momentum extracted by mixed modes in evolved low-mass stars. To this end, we considered 1.3 $M_\odot$ benchmark models of a subgiant (model M0), an early red giant (model M1), and a more evolved red giant (model M2) for which we computed realistic mode amplitudes based on recent CoRoT and *Kepler* observations. We found that mixed modes extract angular momentum in the innermost region of subgiants and red giants. This extraction of angular momentum is found negligible for the subgiant and lower red giant branch models, whereas it is efficient enough to counterbalance the effect of the stellar contraction for the most evolved model.

For this evolved star, mixed modes efficiently transport the angular momentum in the hydrogen-burning shell (that corresponds to the maximum of the buoyancy frequency) but becomes less efficient in the very central layers. We note, however, that mixed modes can be considered as an external torque for meridional circulation (e.g., Mathis et al. 2013). Therefore, such a localized spin-down in the hydrogen-burning shell is likely to feed a strong redistribution of angular momentum in the central layers by meridional circulation. This would nevertheless deserve a quantitative estimate.

Indeed, evolutionary calculations including the effect of mixed modes coupled with meridional circulation and shear instabilities are the next step for a definitive conclusion on the ability of mixed modes to slow down the cores of evolved red giants. Modelling of mode amplitudes would require further investigation since we assumed that the contribution of high-angular degree modes would be negligible due to their high radiative damping. Therefore, we believe that our calculations provide a lower limit. Full non-adiabatic computations would provide more accurate results, however.

We conclude that, for subgiants and early red giants, our results indicate that extraction of angular momentum by mixed modes cannot explain the current observations (Deheuvels et al. 2014). Other physical mechanisms such as internal gravity waves (Talon & Charbonnel 2008; Fuller et al. 2014) or magnetic fields (Rüdiger et al. 2015) should also be present in these stars in order to extract enough angular momentum from the core. In contrast, as demonstrated in this work, the transport of angular momentum by mixed modes is a serious explanation for the observed spin down of the core of evolved stars on the red-giant branch. At least, given the order of magnitude of the induced angular momentum extraction, it seems difficult to neglect this mechanism in the future.

Finally, we note that an extension of this work to central helium burning stars would be desirable in the future. Indeed, even if the mode amplitudes are similar for stars on the vertical branch and on the clump for the same $\nu_{\max}$ (e.g., Mosser et al. 2012a), the maximum of buoyancy frequency is lower and shifted toward higher radius for clump stars (e.g., Montalbán et al. 2013). Therefore, we can expect a lower efficiency of the transport by mixed modes but this needs to be definitively quantified.

Acknowledgements. We acknowledge the ANR (Agence Nationale de la Recherche, France) program IDEE (N° ANR-12-BS05-0008) "Interaction Des Étoiles et des Exoplanètes" as well as financial support from "Programme National de Physique Stellaire" (PNPS) of CNRS/INSU, France. R.M.O. aknowledges funding for the Stellar Astrophysics Centre, provided by The Danish National Research Foundation, and funding for the ASTERISK project (ASTERoseismic Investigations with SONG and *Kepler*) provided by the European Research Council (Grant agreement No. 267864).

Appendix A: Cut-off angular degrees

The cut-off angular degree, $\ell_{\max}$ as introduced in Sect. 4.2, can be defined as the angular degree for which the work performed over an oscillation period through the effect of radiative losses in the inner-most layers becomes of the same order of magnitude as for the work performed in the uppermost layers. More precisely,

$\ell_{\rm max}$ is obtained at $\nu = \nu_{\rm max}$ through the relation

$$(\eta_{\ell_{\rm max}} \mathcal{M}_{\ell_{\rm max}})_{\rm upper\ layers} \approx (\eta_{\ell_{\rm max}} \mathcal{M}_{\ell_{\rm max}})_{\rm inner\ layers}. \quad (A.1)$$

The left-hand side of Eq. (A.1) can be identified with a radial mode of comparable frequency for which the mode mass is computed as described in Sect. 3 and the associated damping rate is obtained using the scaling relation as provided by Belkacem et al. (2012; see also Baudin et al. 2011; Appourchaux et al. 2012). It gives $\eta(\ell = 0, \nu = \nu_{\rm max}) = 2.2\ \mu$Hz for M0, $\eta(\ell = 0, \nu = \nu_{\rm max}) = 0.95\ \mu$Hz for M1, and $\eta(\ell = 0, \nu = \nu_{\rm max}) = 0.06\ \mu$Hz for M2.

The right-hand side of Eq. (A.1) can be identified with a gravity dominated mode for which the mode mass is computed following Sect. 3 and the damping rate is obtained using the asymptotic relation (e.g. Dziembowski et al. 2001; Godart et al. 2009)

$$\eta(\ell_{\rm max}, \nu) = \frac{[\ell_{\rm max}(\ell_{\rm max}+1)]^{3/2}}{8\pi\sigma_{\rm R}^3 \int_0^{R_{\rm c}} k_r\, {\rm d}r} \int_0^{R_{\rm c}} \frac{\nabla_{\rm ad} - \nabla}{\nabla} \frac{\nabla_{\rm ad} N g L}{P r^5}\, {\rm d}r \quad (A.2)$$

where P is the pressure, L is the luminosity, $R_{\rm c}$ is the base of the convective region, $\sigma_{\rm R} = 2\pi\nu$, ∇ is the temperature gradient and $\nabla_{\rm ad}$ its adiabatic counter-part.

Finally, using Eqs. (A.1), and (A.2), one obtains $\ell_{\rm max} = 6$ for M0, $\ell_{\rm max} = 4$ for M1, and $\ell_{\rm max} = 2$ for M2.

References

Aizenman, M., Smeyers, P., & Weigert, A. 1977, A&A, 58, 41
Alexander, D. R., & Ferguson, J. W. 1994, ApJ, 437, 879
Ando, H. 1986, A&A, 163, 97
Angulo, C., Arnould, M., Rayet, M., et al. 1999, Nucl. Phys. A, 656, 3
Appourchaux, T., Benomar, O., Gruberbauer, M., et al. 2012, A&A, 537, A134
Asplund, M., Grevesse, N., & Sauval, A. J. 2005, in Cosmic Abundances as Records of Stellar Evolution and Nucleosynthesis, eds. T. G. Barnes III, & F. N. Bash, ASP Conf. Ser., 336, 25
Baglin, A., Auvergne, M., Barge, P., et al. 2006a, in ESA SP 1306, eds. M. Fridlund, A. Baglin, J. Lochard, & L. Conroy, 33
Baglin, A., Auvergne, M., Boisnard, L., et al. 2006b, in 36th COSPAR Scientific Assembly, COSPAR Meeting, 36, 3749
Baudin, F., Barban, C., Belkacem, K., et al. 2011, A&A, 535, C1
Beck, P. G., Montalban, J., Kallinger, T., et al. 2012, Nature, 481, 55
Bedding, T. R., Mosser, B., Huber, D., et al. 2011, Nature, 471, 608
Belkacem, K., & Samadi, R. 2013, in Lect. Notes Phys., 865, eds. M. Goupil, K. Belkacem, C. Neiner, F. Lignières, & J. J. Green (Berlin: Springer Verlag), 179
Belkacem, K., Dupret, M. A., Baudin, F., et al. 2012, A&A, 540, L7
Belkacem, K., Marques, J. P., Goupil, M. J., et al. 2015, A&A, 579, A30
Benomar, O., Belkacem, K., Bedding, T. R., et al. 2014, ApJ, 781, L29
Borucki, W. J., Koch, D., Basri, G., et al. 2010, Science, 327, 977
Cantiello, M., Mankovich, C., Bildsten, L., Christensen-Dalsgaard, J., & Paxton, B. 2014, ApJ, 788, 93
Canuto, V. M., Goldman, I., & Mazzitelli, I. 1996, ApJ, 473, 550
Ceillier, T., Eggenberger, P., García, R. A., & Mathis, S. 2013, A&A, 555, A54
Chaplin, W. J., & Miglio, A. 2013, ARA&A, 51, 353
Christensen-Dalsgaard, J. 2008, Ap&SS, 316, 113
Christensen-Dalsgaard, J. 2011, Astrophysics Source Code Library [record ascl:1109.002]
Deheuvels, S., García, R. A., Chaplin, W. J., et al. 2012, ApJ, 756, 19
Deheuvels, S., Doğan, G., Goupil, M. J., et al. 2014, A&A, 564, A27
Dupret, M.-A., Belkacem, K., Samadi, R., et al. 2009, A&A, 506, 57
Dziembowski, W. A. 1971, Acta Astron., 21, 289
Dziembowski, W. A., Gough, D. O., Houdek, G., & Sienkiewicz, R. 2001, MNRAS, 328, 601
Eggenberger, P., Montalbán, J., & Miglio, A. 2012, A&A, 544, L4
Fuller, J., Lecoanet, D., Cantiello, M., & Brown, B. 2014, ApJ, 796, 17
Godart, M., Noels, A., Dupret, M.-A., & Lebreton, Y. 2009, MNRAS, 396, 1833
Goupil, M. J., Mosser, B., Marques, J. P., et al. 2013, A&A, 549, A75
Grosjean, M., Dupret, M.-A., Belkacem, K., et al. 2014, A&A, 572, A11
Iglesias, C. A., & Rogers, F. J. 1996, ApJ, 464, 943
Imbriani, G., Costantini, H., Formicola, A., et al. 2004, A&A, 420, 625
Lee, U., & Saio, H. 1993, MNRAS, 261, 415
Maeder, A. 2009, Physics, Formation and Evolution of Rotating Stars, Astronomy and Astrophysics Library (Berlin, Heidelberg: Springer)
Maeder, A., & Meynet, G. 2014, ApJ, 793, 123
Maeder, A., & Zahn, J.-P. 1998, A&A, 334, 1000
Marques, J. P., Goupil, M. J., Lebreton, Y., et al. 2013, A&A, 549, A74
Mathis, S., & Zahn, J.-P. 2004, A&A, 425, 229
Mathis, S., Decressin, T., Eggenberger, P., & Charbonnel, C. 2013, A&A, 558, A11
Michel, E., Baglin, A., Auvergne, M., et al. 2008, Science, 322, 558
Montalbán, J., Miglio, A., Noels, A., et al. 2013, ApJ, 766, 118
Mosser, B., Belkacem, K., Goupil, M., et al. 2010, A&A, 517, A22
Mosser, B., Barban, C., Montalbán, J., et al. 2011, A&A, 532, A86
Mosser, B., Elsworth, Y., Hekker, S., et al. 2012a, A&A, 537, A30
Mosser, B., Goupil, M. J., Belkacem, K., et al. 2012b, A&A, 548, A10
Mosser, B., Benomar, O., Belkacem, K., et al. 2014, A&A, 572, L5
Rogers, F. J., Swenson, F. J., & Iglesias, C. A. 1996, ApJ, 456, 902
Rüdiger, G., Gellert, M., Spada, F., & Tereshin, I. 2015, A&A, 573, A80
Samadi, R. 2011, in Lect. Notes Phys. 832, eds. J.-P. Rozelot, & C. Neiner (Berlin: Springer Verlag), 305
Samadi, R., Belkacem, K., Dupret, M.-A., et al. 2012, A&A, 543, A120
Scuflaire, R. 1974, A&A, 36, 107
Talon, S., & Charbonnel, C. 2008, A&A, 482, 597